Multiplex Fluorescent, Activity-Based Protein Profiling Identifies Active α-Glycosidases and Other Hydrolases in Plants[1][OPEN]

Amjad M. Husaini,[a,f] Kyoko Morimoto,[a] Balakumaran Chandrasekar,[a] Steven Kelly,[a] Farnusch Kaschani,[b] Daniel Palmero,[c] Jianbing Jiang,[d] Markus Kaiser,[b] Oussama Ahrazem,[e] Hermen S. Overkleeft,[d] and Renier A. L. van der Hoorn[a,2]

[a]Department of Plant Sciences, University of Oxford, Oxford OX1 3RB, United Kingdom
[b]Chemische Biologie, Zentrum für Medizinische Biotechnologie, Fakultät für Biologie, Universität Duisburg-Essen, 45117 Essen, Germany
[c]Universidad Politécnica de Madrid, Escuela Técnica Superior de Ingenieria Agronómica, Alimentaria cv de Biosistemas, Ciudad Universitaria s/n, 28040 Madrid, Spain
[d]Gorlaeus Laboratories, Leiden Institute of Chemistry and Netherlands Center for Proteomics, 2333 CC Leiden, The Netherlands
[e]Instituto Botánico, Facultad de Farmacia, Universidad de Castilla-La Mancha, Campus Universitario s/n, Albacete 02071, Spain
[f]Sher-e-Kashmir University of Agricultural Sciences and Technology of Kashmir, Shalimar- 190025, Jammu and Kashmir, India

ORCID IDs: 0000-0003-1293-3118 (A.M.H.); 0000-0001-8583-5362 (S.K.); 0000-0002-1442-1274 (D.P.); 0000-0003-4792-8140 (J.J.); 0000-0001-9183-9319 (O.A.); 0000-0002-3692-7487 (R.A.L.v.d.H.).

With nearly 140 α-glycosidases in 14 different families, plants are well equipped with enzymes that can break the α-glucosidic bonds in a large diversity of molecules. Here, we introduce activity-based protein profiling (ABPP) of α-glycosidases in plants using α-configured cyclophellitol aziridine probes carrying various fluorophores or biotin. In Arabidopsis (*Arabidopsis thaliana*), these probes label members of the GH31 family of glycosyl hydrolases, including endoplasmic reticulum-resident α-glucosidase-II Radial Swelling3/Priority for Sweet Life5 (RSW3/PSL5) and Golgi-resident α-mannosidase-II Hybrid Glycosylation1 (HGL1), both of which trim *N*-glycans on glycoproteins. We detected the active state of extracellular α-glycosidases such as α-xylosidase XYL1, which acts on xyloglucans in the cell wall to promote cell expansion, and α-glucosidase AGLU1, which acts in starch hydrolysis and can suppress fungal invasion. Labeling of α-glycosidases generates pH-dependent signals that can be suppressed by α-glycosidase inhibitors in a broad range of plant species. To demonstrate its use on a nonmodel plant species, we applied ABPP on saffron crocus (*Crocus sativus*), a cash crop for the production of saffron spice. Using a combination of biotinylated glycosidase probes, we identified and quantified 67 active glycosidases in saffron crocus stigma, of which 10 are differentially active. We also uncovered massive changes in hydrolase activities in the corms upon infection with *Fusarium oxysporum* using multiplex fluorescence labeling in combination with probes for serine hydrolases and cysteine proteases. These experiments demonstrate the ease with which active α-glycosidases and other hydrolases can be analyzed through ABPP in model and nonmodel plants.

Carbohydrates in the form of glycoproteins, polysaccharides, and glycolipids play significant roles in cell physiology and the development of plants, animals, and microbes. The enzymes that cleave and build the glycosidic bonds of glycoconjugates, oligosaccharides, and polysaccharides act on some of the most structurally diverse substrates in nature. Based on amino acid sequence similarity, these carbohydrate-active enzymes are classified into over 200 families of glycosidases, glycosyltransferases, carbohydrate esterases, and polysaccharide lyases in the Carbohydrate-Active Enzymes database (Coutinho and Henrissat, 1999).

Enzymes that catalyze the synthesis and breakdown of glycosidic bonds account for 1% to 3% of the proteins encoded by the genomes of most organisms. For instance, the genome of Arabidopsis (*Arabidopsis thaliana*) encodes for 400 glycosidases. These glycosidases play critical roles ranging from the biosynthesis of glycoproteins to the digestion and decomposition of polysaccharides. The α-glycosidases are an important subset of these enzymes. The Carbohydrate-Active Enzymes database counts 138 α-glycosidases for Arabidopsis, subdivided into 14 families based on sequence homology (Lombard et al., 2014). These include α-galactosidases, α-amylases, α-xylosidases, α-rhamnosidases, α-fucosidases, α-threhalases, α-mannosidases, α-arabinofuranosidases, and α-glucosidases.

The Glycosyl Hydrolase31 (GH31) family contains important α-glycosidases that act across the plant kingdom in protein *N*-glycosylation (Radial Swelling3

[RSW3] and Hybrid Glycosylation1 [HGL1]), cell wall modulation (XYL1), and starch degradation (AGLU1). All GH31 family members retain α-glycosidases that retain the stereocenter of the C1 atom of the substrate with relatively large molecular mass values (~100 kD). Other α-glycosidases can be found in 13 additional GH families. Most of these glycosidases are inverting enzymes that invert the stereocenter of the C1 atom in the substrate. GH63, for example, contains the inverting α-glucosidase-I (GCS1; KNOPF), which resides in the endoplasmic reticulum, and removes the first Glc from the *N*-glycan of glycoproteins (Boisson et al., 2001). Plant α-glycosidases can have interesting properties. For instance, some α-glycosidases mediate the release of monoterpenoid aroma in apricot (*Prunus armeniaca*; Krammer at al., 2002). Furthermore, the α-glycosidase of the hyperthermophilic archaebacterium *Pyrococcus furiosus* remains active at 105°C to 115°C (Costantino et al., 1990).

Many α-glycosidases can be blocked by selective inhibitors. Compounds like miglitol and acarbose are well-described α-glucosidase inhibitors used as antidiabetic drugs (Hillman et al., 1989; Carrascosa et al., 2001). These compounds have occasionally been used to conduct research in plants; for instance, α-amylase was inhibited to study barley (*Hordeum vulgare*) seed germination (Frandsen et al., 2000; Stanley et al., 2011). Iminosugars also have been used to study plant cell wall metabolism and starch remobilization (Andriotis et al., 2016).

The large number of α-glycosidases, their complex regulation, and their varied subcellular localization call for new tools to detect when and where these enzymes are active. Activity-based protein profiling (ABPP) is a simple and widely applicable technique that can display active enzymes in crude extracts and living tissues (Cravatt et al., 2008). ABPP is based on the use of small chemical probes that mimic a substrate but lock the enzymatic mechanism in the covalent intermediate state, labeling only active enzymes. Fluorescent probes facilitate the detection of the labeled proteome on protein gels by fluorescence scanning, whereas biotinylated probes facilitate the purification and identification of labeled proteins by mass spectrometry (MS).

ABPP technology was initially developed in medical biology (Verhelst and Bogyo, 2005; Cravatt et al., 2008; Willems et al., 2014) and is used increasingly in microbiology (Sadler and Wright, 2015) and plant biology (Morimoto and van der Hoorn, 2016). For instance, we have used activity-based probes to study the activities of the proteasome, Ser hydrolases, Cys proteases, glutathione transferases, aldehyde hydrogenases, metalloproteases, and ATP-binding proteins in plants (Kaschani et al., 2009; Gu et al., 2010, 2013; Kolodziejek et al., 2011; Lenger et al., 2012; Richau et al., 2012; Misas-Villamil et al., 2013, 2017; Stiti et al., 2016). These probes also have been used by other plant research laboratories to investigate maize (*Zea mays*) smut effectors, herbicide activation, wheat (*Triticum aestivum*) leaf senescence, and apical dominance in potato (*Solanum tuberosum*) tubers (Gershater et al., 2007; Martínez et al., 2007; Mueller et al., 2013; Teper-Bamnolker et al., 2017).

We previously validated activity-based probes for retaining β-glycosidases in plants (Chandrasekar et al., 2014). Using β-configured cyclophellitol aziridine probes, we were able to monitor the activity of dozens of β-glycosidases, including β-myrosinases, β-glucosidases, β-xylosidases, and β-galactosidases (Chandrasekar et al., 2014). Here, we validate the use of α-configured cyclophellitol aziridine probes for retaining α-glycosidases in plants. These probes were recently developed and tested on mammalian proteomes (Jiang et al., 2016). We characterize the labeling profile, identify labeled proteins, and characterize the inhibitor sensitivity of labeling. We also show their broad applicability for studying glycosidases in nonmodel plant species, exemplified by saffron crocus (*Crocus sativus*), and demonstrate their use in combination with other fluorescent probes for profiling multiple classes of hydrolase activities simultaneously.

RESULTS

Distinct Activity-Based Probes for α- and β-GHs

We studied the labeling of three different activity-based probes that carry a cyclophellitol aziridine reactive group with glucopyranose in the α-configuration (Fig. 1A). This reactive group has been designed to target retaining α-glucoside hydrolases (αGHs; Jiang et al., 2016). The three probes used differ only in the reporter tag: JJB382 carries a Bodipy(FL) fluorophore, JJB383 carries a Cy5 fluorophore, and JJB384 carries a biotin affinity tag (Supplemental Fig. S1). These probes are distinct from the probes introduced earlier, which contained β-configured cyclophellitol aziridine reactive groups, aimed at labeling β-glucoside hydrolases (βGHs; Kallemeijn et al., 2012; Chandrasekar et al., 2014). The β-configured probes carry different reporter tags: KY371 carries an alkyne minitag, JJB70 carries a Bodipy(FL) fluorophore, JJB75 carries a Bodipy(TMR) fluorophore, and JJB111 carries a biotin affinity tag

[1] This work was supported by Department of Biotechnology of the Government of India (A.M.H.), ERC Consolidator grant 616449 GreenProteases (R.A.L.v.d.H.), John Fell Fund (K.M.), ERC starting grant (M.K., grant no. 258413), the Deutsche Forschungsgemeinschaft (M.K., grant no. INST 20876/127-1 FUGG), and the China Scholarship Council (J.J., grant no. 2011618045).

[2] Address correspondence to renier.vanderhoorn@plants.ox.ac.uk.

The author responsible for distribution of materials integral to the findings presented in this article in accordance with the policy described in the Instructions for Authors (www.plantphysiol.org) is: Renier A.L. van der Hoorn (renier.vanderhoorn@plants.ox.ac.uk).

A.M.H., K.M., B.C., and R.A.L.v.d.H. designed the research; A.M.H., K.M., and B.C. performed research; D.P. and O.A. provided *Fox*-infected corms; F.K. and M.K. performed MS analysis; J.J. and H.S.O. contributed new analytic tools; S.K. generated the saffron proteome database; A.M.H., K.M., B.C., and F.K. analyzed data; R.A.L.v.d.H. wrote the article with input from all authors.

[OPEN] Articles can be viewed without a subscription.

www.plantphysiol.org/cgi/doi/10.1104/pp.18.00250

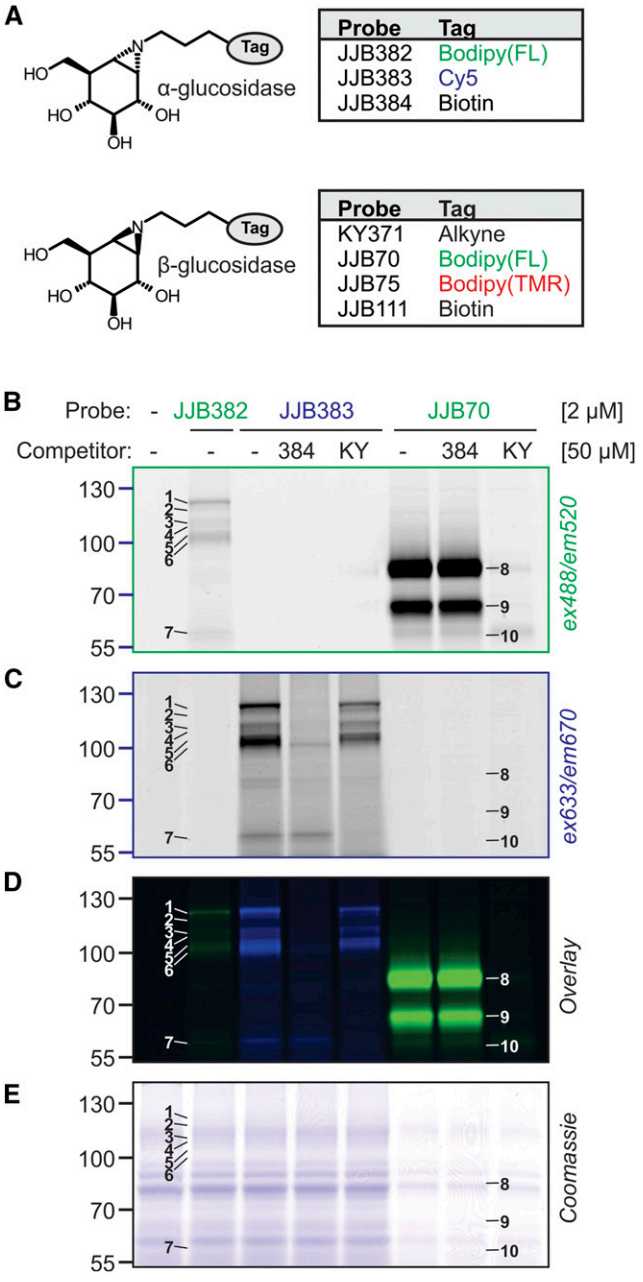

Figure 1. α-Glucosidase probes label distinct proteins in Arabidopsis leaf extracts. A, Structures of the probes used for α-glucosidases (top) and β-glucosidases (bottom). For the detailed structures, see Supplemental Figure S1. B to E, Activity profiles of α- and β-glucosidase probes. Arabidopsis leaf extracts at pH 7 were preincubated with or without 50 μM JJB384 (384) or KY371 (KY) for 30 min and then labeled with or without 2 μM JJB382, JJB383, or JJB70 for 1 h. Proteins were separated on protein gels and analyzed by in-gel fluorescence scanning at excitation 488 nm and emission 520 nm (ex488/em520; B) or ex633/em670 (C), overlaid (D), and Coomassie Blue stained (E). Four times less JJB70-labeled sample was loaded to compare JJB70 and JJB382 profiles. For full gels, see Supplemental Figure S2.

(Fig. 1A). When we previously tested these β-configured probes in plants, we found that they labeled a broad range of βGHs of the GH1, GH3, GH5, GH30, GH35, GH51, GH52, and GH79 families but not αGHs from GH31 (Chandrasekar et al., 2014).

The α-Glucosidase Probes Label a Distinct Subproteome

To test the labeling by the new probes, Arabidopsis leaf extracts were labeled with JJB382 and JJB70, which differ in their reactive group configuration but have the same fluorophore. Labeled proteomes were separated on protein gels and detected by in-gel fluorescence scanning. The labeling profile of JJB382 is notably distinct from that described earlier for JJB70. While JJB70 generates two strong signals at 70 kD, caused by the myrosinases TGG1 and TGG2 (Chandrasekar et al., 2014), JJB382 labeling does not display these signals. Instead, JJB382 labeling generates six signals (signals 1–6) at 100 to 130 kD (Fig. 1B; Supplemental Fig. S2). These JJB382 signals 1 to 6 are 20-fold weaker than the JJB70 signals 8 and 9; therefore, high protein loading is required to detect the JJB382 signals robustly (Fig. 1, B and E). Both JJB70 and JJB382 labeling also display a signal at 60 kD (signal 7; Fig. 1B). Labeling with JJB382 causes a profile that seems identical to that of JJB383, indicating that the different fluorophores do not affect labeling (Fig. 1C).

Next, we tested the specificity of labeling in competition experiments. JJB383 labeling of signals 1 to 6 is suppressed upon preincubation with an excess of α-configured JJB384 but not β-configured KY371, indicating that signals 1 to 6 represent αGHs (Fig. 1C). However, JJB383 labeling of signal 7 is suppressed upon preincubation with β-configured KY371 but not α-configured JJB384, suggesting that this is a βGH-derived signal (Fig. 1C). Taken together, these experiments indicate that the α-configured fluorescent probes label a distinct set of proteins when compared with the β-configured probes.

Multiplex Labeling of α- and β-Glycosidases

Prelabeling with β-configured JJB75 does not affect the labeling of signals 1 to 6 by α-configured JJB382 at 100 to 130 kD (Supplemental Fig. S3A). However, JJB382 signal 7 at 60 kD is suppressed upon prelabeling with β-configured JJB75, consistent with this signal being generated by a βGH. Indeed, JJB75 labeling also generates a 60-kD signal, similar to signal 10 of β-configured JJB70 (Supplemental Fig. S3, B and D). Prelabeling with JJB75 also generates an additional signal 8 at 70 kD (Supplemental Fig. S3A), which might result from unintended excitation of JJB75 at 488 nm. JJB75-labeled proteins also are excited by the 633-nm laser (Supplemental Fig. S3C), indicating that JJB75 cannot be used for colabeling.

Conversely, prelabeling with α-configured JJB383 does not affect β-configured JJB70 labeling (Supplemental Fig. S3A). The labeling profile of JJB383 (Supplemental Fig. S3A) also is identical to that of JJB382 (Supplemental Fig. S3A), except for the absence of signal 7, consistent

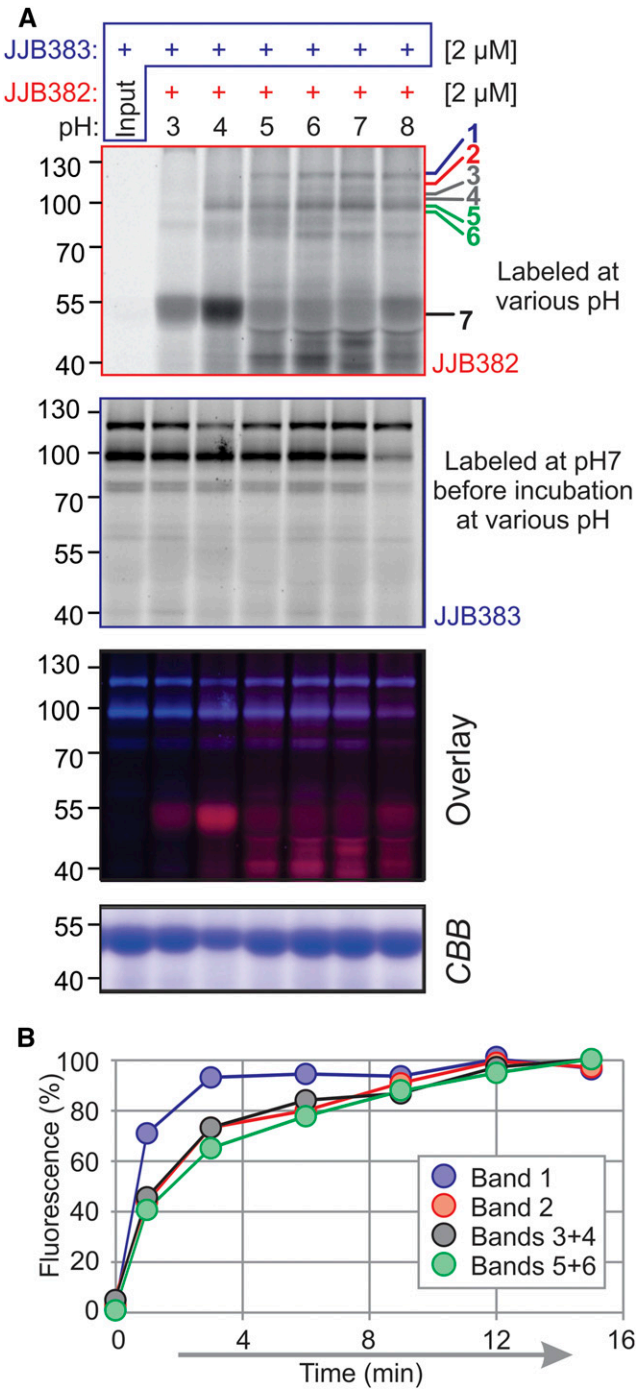

Figure 2. pH dependence and time course of α-glucosidase labeling. A, Arabidopsis leaf extracts were labeled with 2 μM JJB383 for 1 h at pH 7. This sample was buffer exchanged with water, followed by mixing with an unlabeled proteome plus 2 μM JJB383, and labeled for 1 h at various pH values. Proteins were precipitated with acetone and analyzed by in-gel fluorescence scanning at ex488/em520 for JJB382 (top gel), ex633/em670 for JJB383 (second gel), and Coomassie Blue (CBB) staining (bottom gel). The overlay (third gel) shows JJB382 in red and JJB383 in blue. B, Quantified time course of α-glucosidase labeling of Arabidopsis leaf extracts. Arabidopsis leaf extracts were labeled with 2 μM JJB383 at pH 7, and samples were collected at various time points. The *y* axis displays fluorescence intensities from protein gels, and the *x* axis indicates time (minutes).

with it being a βGH labeled by JJB70. Taken together, these data demonstrate that the α-configured probes cause distinct signals at 100 to 130 kD and that probes having different fluorophores can be used for colabeling. Also, all fluorophores except for the Bodipy(TMR) of JJB75 are detected selectively using distinctive excitation and emission wavelengths.

The α-Glycosidases Have Distinct Labeling Characteristics

The labeling experiments presented so far were performed at pH 7. Because α-glucosidases act in different subcellular locations with specific microenvironments, we tested labeling at various pH levels. JJB383 labeling is strongly pH dependent. Labeling of signals 1 to 5 occurs only at pH 6 to 8, while labeling of signal 6 also occurs at pH 5 to 9 (Fig. 2A; Supplemental Fig. S4A). In addition, signal 7 is most intense at pH 5, indicating that these βGHs act at acidic pH (Fig. 2A; Supplemental Fig. S4A). The αGH-derived signals 1 to 5, however, are best labeled at neutral and slightly acidic pH (pH 6–8). To investigate whether the reduced αGH signals observed at low pH are caused by protein precipitation or degradation, we incubated a sample that was prelabeled at pH 7 with JJB383 at various pH values. JJB383-labeled proteins were unaffected upon incubation at low pH (Fig. 2A, JJB383), illustrating that αGH labeling is pH dependent. Therefore, we focused further on α-glycosidase labeling at pH 7.

Next, we investigated the timing of JJB383 labeling. Signals 1 to 6 appear upon labeling within minutes and reach their maximum within 12 min (Fig. 2B). Signal 1, however, intensifies faster, indicating that this αGH has a higher turnover rate and is labeled faster by JJB383.

α-Glucosidase Inhibitors Selectively Block Labeling

To confirm that the 100- to 130-kD signals are generated by α-glucosidases, we tested labeling upon incubation with known α-glucosidase and control inhibitors. We tested two commercially available α-glucosidase inhibitors, acarbose and miglitol, which are used as antidiabetic drugs (Hillman et al., 1989; Carrascosa et al., 2001). We also included the β-galactosidase inhibitor galactostatin and three iminosugars that mimic Glc but differ stereochemically at the 5′ and 4′ positions: 1-deoxynojirimycin (DNJ), 1-deoxygalactonojirimycin (DGJ; migalastat), and *ido*-1-deoxynojirimycin (*ido*DNJ; Fig. 3A).

Preincubation with miglitol suppresses JJB383 labeling of signals 1 to 6 (Fig. 3B), indicating that these signals are caused by α-glycosidases. Surprisingly, acarbose does not affect the labeling of signal 1 but suppresses the labeling of signals 2 to 6 (Fig. 3B). Galactostatin is unable to prevent JJB383 labeling, indicating the relevance of the stereochemistry at the 1′ and 4′ positions (Fig. 3B). Of the

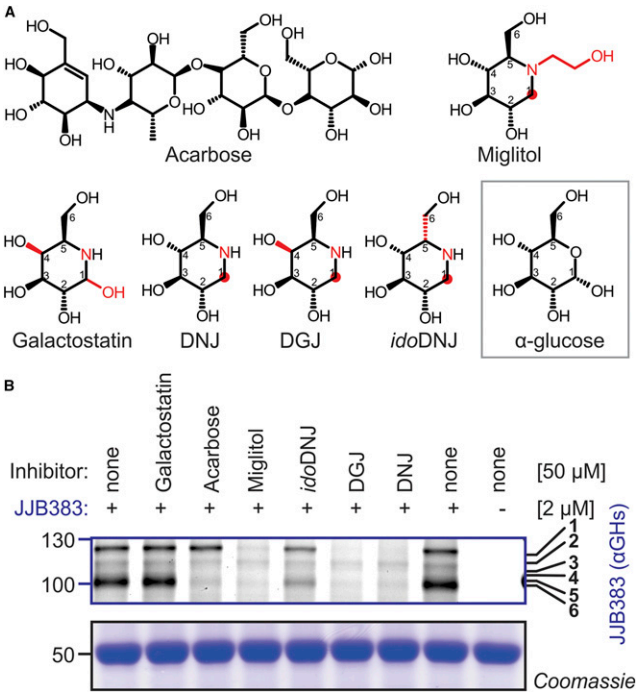

Figure 3. JJB383 labeling is blocked by α-glucosidase inhibitors. A, Glycosidase inhibitors used in this study. B, Competitive ABPP using glycosidase inhibitors. Arabidopsis leaf extracts were preincubated with and without 50 μM inhibitors and labeled with 2 μM JJB383 for 1 h at pH 7. Samples were analyzed by in-gel fluorescence scanning (ex633/em670; top gel) and Coomassie Blue staining (bottom gel).

tested iminosugars, DNJ and DGJ effectively block JJB383 labeling (Fig. 3B), indicating that the 4′ stereochemistry is not essential for inhibiting JJB383 labeling. By contrast, *ido*DNJ is unable to block JJB383 labeling, indicating that the stereochemistry at the 5′ position is essential for inhibiting JJB383 labeling. These results demonstrate that labeling of the 100- to 130-kD proteins with α-configured probes is highly selective.

The 100- to 130-kD Signals Contain Four α-Glycosidases

To identify the signals, we labeled Arabidopsis leaf extracts at pH 7 with biotinylated α-configured JJB384. We purified the biotinylated proteins and analyzed them by in-gel and on-bead digestion. For the in-gel digestion procedure, purified JJB384-labeled proteins were separated on protein gels and stained with Sypro Ruby. Signals 1 to 6 that appear at 100 to 130 kD in the JJB384-labeled sample, but not in the no-probe control, were excised and in-gel digested with trypsin (Fig. 4A). Released tryptic peptides were identified by LC-MS/MS. Four α-glycosidases were identified from all three excised signals: RSW3/PSL5 (Priority for Sweet Life5 [At5g63840]; 36 spectral counts), α-xylosidase XYL1 (At1g68560; 17 spectral counts), HGL1 (At3g23640; 12 spectral counts), and α-glucosidase-1 AGLU1 (At5g11720; 10 spectral counts; Fig. 4B). These four enzymes are GH31 α-glycosidases, and their predicted molecular masses are 104, 102, 111, and 101 kD, respectively (Fig. 4C). These proteins can run at higher molecular mass because they are likely *N*-glycosylated, as they have two, nine, three, and nine putative *N*-glycosylation sites, respectively (Fig. 4C). We also identified a few peptides from the β-glucosidase BGLC3 (At5g04885; two spectral counts) from signals 4 to 6 (Fig. 4A, bands 4 and 5). However, this protein has a predicted molecular mass of 68 kD and might be a contaminant from a different region of the gel.

Biotinylated α-Glycosidase Probes Label 12 Different α- and β-Glycosidases

We also performed on-bead digestion to detect biotinylated proteins and to determine if more proteins are labeled by JJB384. The pulldown was performed three times for JJB384-labeled proteins and three times for the no-probe control. Of the 388 proteins detected, 33 were not from Arabidopsis and 194 were not detected in more than two of the six samples (Fig. 5A). The average label-free quantification (LFQ) intensities for the 161 remaining proteins were plotted against their average distribution between the no-probe control and the JJB384 samples. As usual, the most abundant proteins were the endogenous biotinylated proteins BCCP, MCCA, and ACC1 as well as the highly abundant large Rubisco subunit RBCL (Fig. 5B, top signals). We also detected 12 proteins nearly exclusively in the JJB384 sample (Fig. 5B, right side), which are all glycosidases (Fig. 5C). We detected the same four GH35 α-glucosidases as with in-gel digestion: AGLU11, XYL1, HGL1, and RSW3. These four α-glucosidases are detected with high LFQ intensities and protein coverage, consistent with them being the preferred targets of JJB384. The remaining glycosidases are β-glycosidases of families GH116 (At4g10060), GH1 (BGLU15, BGLU40, BGLU42, and BGLU44), and GH3 (F13I12, BGLC1, and BGLC2; Fig. 5C). The high spectral counts for BGLU44 and BGLC1 and their predicted molecular masses suggest that these proteins might underlie signal 7, possibly mixed with other GH1 and GH3 enzymes. By contrast, our earlier pull-down analysis with β-configured JJB111 displayed most of the detected β-glycosidases but none of the α-glucosidases (Fig. 5C, right). In conclusion, although JJB384 preferentially targets α-glucosidases, it also labels some but not all β-glycosidases. TGG1 and TGG2, for example, are abundant GH1 glucosidases in leaves but were not detected among JJB384-labeled proteins.

Profiling of Active α-Glucosidases Can Be Applied to Other Plant Species

We next tested whether the α-configured probes can be used to detect α-glucosidases in leaf extracts of other plant species. In addition to Arabidopsis, we included a model legume (alfalfa [*Medicago sativa*]), two solanaceous plants (*Nicotiana benthamiana* and tomato [*Solanum*

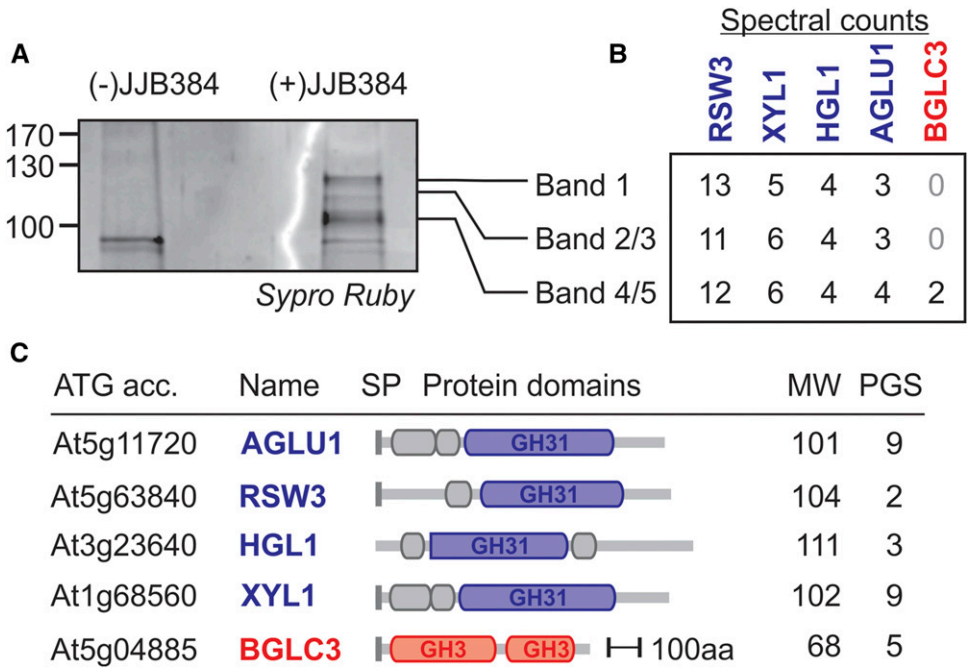

Figure 4. The 100- to 130-kD region contains four α-glucosidases. A, Arabidopsis leaf extracts were labeled with and without 5 μM JJB384 for 1 h at pH 7. Biotinylated proteins were purified on high-capacity streptavidin agarose resin beads and eluted by boiling in SDS sample buffer. Proteins were separated on protein gels and stained with Sypro Ruby. Gel slices were excised and treated with trypsin, and released peptides were analyzed by liquid chromatography-tandem mass spectrometry (LC-MS/MS). B, Five glycosidase proteins were identified in bands 1 to 6. C, Detected proteins and their domain structure, predicted molecular mass (MW; in kD), and number of putative *N*-glycosylation sites (PGS). aa, Amino acids.

lycopersicum]), two monocots (rice [*Oryza sativa*) and maize), and a gymnosperm (sago palm [*Cycas revoluta*]). Preincubation with 50 μM miglitol was used to distinguish between α- and β-glucosidases. Labeling causes fluorescent signals at 10 to 130 kD for all the plant species tested; these signals are suppressed upon miglitol preincubation and absent in the no-probe control (Fig. 6). The signals are similar in intensity and molecular mass, although there are slight differences in the profiles. Signals at 40 to 60 kD are not suppressed upon preincubation with miglitol, indicating that these are generated by β-glucosidases (Fig. 6). In conclusion, these α-configured probes can be used to monitor miglitol-sensitive α-glucosidases in various plant species.

Glycosidase Activity Profiling of a Nonmodel: Saffron Crocus Anthesis

We next used glycosidase activity profiling to investigate anthesis in saffron crocus. The stigmas of these monocot flowers are harvested, dried, and used widely as a spice and for food coloring (Ahrazem et al., 2015). During the drying process, heat, and presumably glucosidases, convert the bitter-tasting picrocrocin into Glc and safranal, which gives saffron its distinct aroma (Jain et al., 2016). The glycosidases catalyzing this reaction, and the conversion of other volatiles and nonvolatile apocarotenoids, have not been identified.

To initiate the characterization of safranal-generating glucosidases, we performed glucosidase activity profiling at two different stages of stigma development and maturation: yellow (stage 1) and scarlet (stage 4; Wafai et al., 2015). Taking advantage of having different fluorophores on α- and β-configured probes, we simultaneously monitored active α- and β-glucosidases using multiplex fluorescence. As with other plant species, the α-configured probe JJB383 displays signals at 100 to 130 kD, which do not change in intensity during anthesis (Fig. 7A). By contrast, the β-configured JJB70 displays a constant signal at 70 kD and a differential signal at 110 kD that is particularly strong at stage 4 (Fig. 7A). This 110-kD signal overlaps with the JJB383-derived signals, causing a purple signal in the overlay image (Fig. 7A).

To determine if the 110-kD glycosidase is labeled by both JJB383 and JJB70, or if these signals are generated by two different labeled glycosidases that comigrate, we preincubated the samples with the αGH inhibitor miglitol and the βGH inhibitor KY371. The JJB70-labeled 110-kD signal is only suppressed by KY371, and the JJB383-labeled signals are only suppressed by miglitol (Fig. 7A). This result demonstrates that the labeled GHs are comigrating and that the differential signal is a βGH.

To identify glucosidases that are differentially active between stages 1 and 4, we performed labeling with mixed, biotinylated probes targeting both α- and β-glycosidases (JJB384 and JJB111, respectively). Labeling was performed on three biological replicates, both from stage 1 and 4 samples, and peptides from on-bead trypsin digestion were identified. To facilitate the annotation of MS spectra, we annotated the proteome based on published RNA sequencing data of saffron crocus (Jain et al., 2016). We detected and quantified 67 putative glycosidases (Fig. 7B) and plotted their relative occurrence in stages 1 and 4 against the predicted molecular masses (Fig. 7B).

Four of the detected glycosidases are putative orthologs of Arabidopsis XYL1, RSW3, and AGLU1 of the GH31 family. However, these αGHs are not

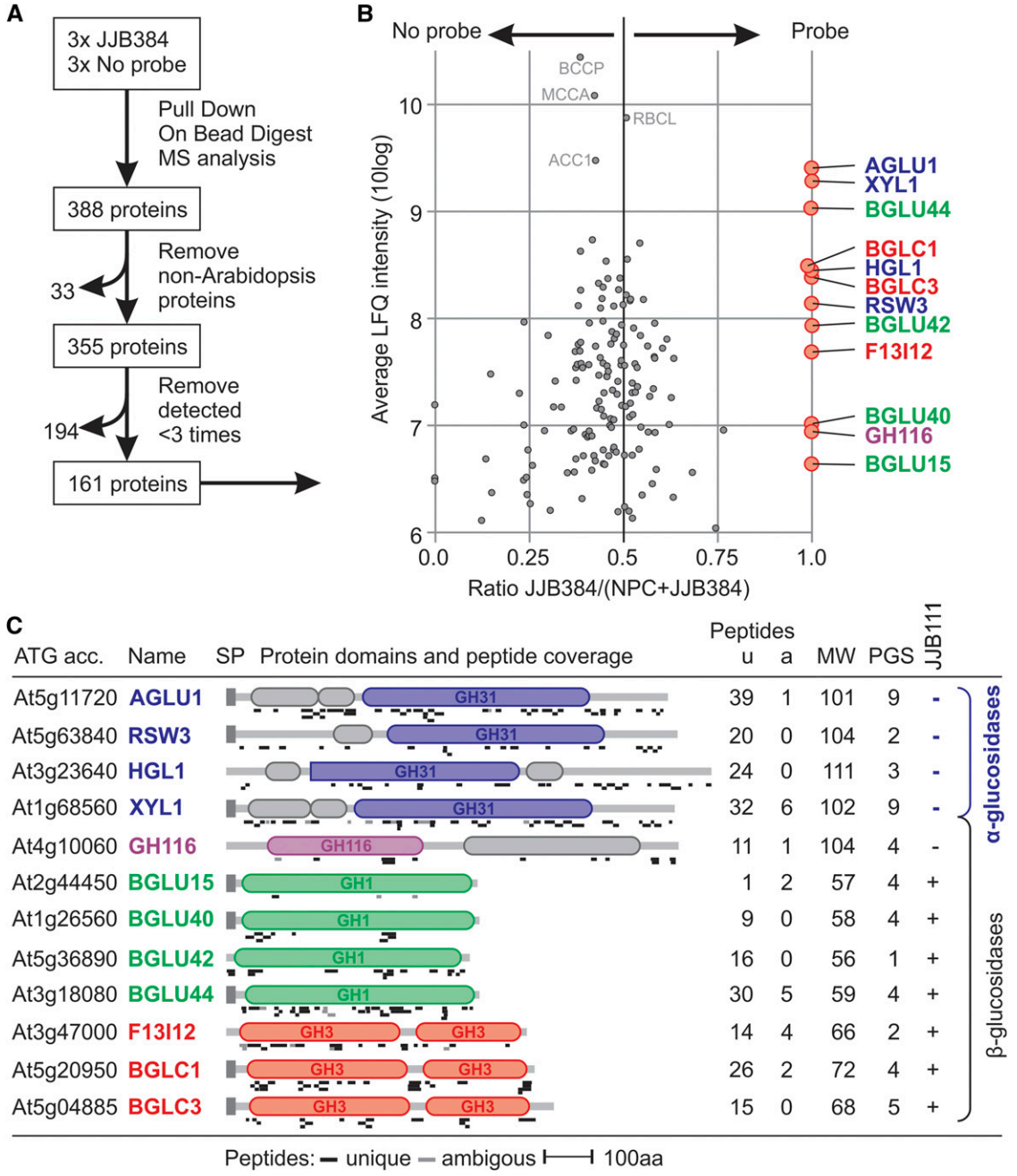

Figure 5. On-bead digestion identifies 12 α- and β-glycosidases. A, Selection criteria for pull-down proteomics. Arabidopsis leaf extracts were labeled with and without 5 μM JJB384, and biotinyated proteins were purified on high-capacity streptavidin agarose resin beads. On-bead digests with trypsin were analyzed by MS, and Arabidopsis proteins that were detected in three of the six pull-down experiments were selected. B, Distribution of the detected proteins over the no-probe control (NPC) and the JJB384-labeled sample. The average LFQ scores were plotted against the distribution of the LFQ scores for each protein detected with and without the probe. All 12 highly enriched proteins are glycosidases, highlighted on the right. Abundant, nonenriched signals come from endogenously biotinylated proteins (BCCP, MCCA, and ACC1) and the large subunit of Rubisco (RBCL). C, Characterization of the detected probe targets. We detected four GH1 glycosidases (green), three GH3 glycosidases (red), four GH31 glycosidases (blue), and one GH116 glycosidase (purple), each with unique (black) and ambiguous (gray) peptides, summarized in columns u and a, respectively. The presence of a signal peptide (SP; SignalP prediction), the predicted molecular mass (MW; in kD), and number of putative *N*-glycosylation sites (PGS; NxS/T) are indicated. α/β, Annotation as α- or β-glycosidase; aa, amino acids; JJB111, detected previously in β-glycosidase pulldowns (Chandrasekar et al., 2014).

differentially active (Fig. 7B, blue circles), consistent with the unaltered fluorescence labeling profiles (Fig. 7A). In addition to GH31 glycosidases, we also detected peptides from representatives of nine additional GH families: GH1 (21×), GH35 (15×), GH3 (12×), GH116 (10×), GH31 (4×), GH17 (2×), GH2 (1×), GH5 (1×), and GH27 (1×).

Of the 67 active glycosidases that we could quantify, eight were significantly up-regulated more than 2-fold in stage 4 stigmas (Fig. 7B, right, encircled), including three GH3, three GH35, two GH116, and one GH1. One GH1 glycosidase with a predicted molecular mass of 130 kD was significantly down-regulated more than 2-fold when compared with stage 4 stigmas (Fig. 7B, left, encircled). We also note the enrichment of several additional GH1 glycosidases in stage 4 stigmas, albeit not statistically significant (Fig. 7B, green circles). The differential 110-kD βGH detected with JJB70 labeling is likely the GH116 enzyme CsTc017194, because this enzyme has a predicted molecular mass of 106 kD and is 4.5-fold up-regulated in stage 4 stigmas (Fig. 7B, left top purple circle). This experiment illustrates the power of applying quantitative glycosidase activity profiling on nonmodel plant species.

Multiplex Activity Profiling Displays Changed Hydrolase Activities in *Fusarium oxysporum*-Infected Corms

To illustrate the combination of glycosidase activity profiling with activity profiling of other enzyme classes, we investigated infections of saffron corms with *Fusarium oxysporum* (*Fox*). *Fusarium* corm rot caused by *Fox* is the most destructive disease in saffron, having caused severe yield losses in saffron-producing countries (Cappelli, 1994; Husaini, 2014). Saffron crocus corms were infected with four different *Fox* isolates, including three different *formae speciales* (Palmero et al., 2014), and analyzed for differential protein activities at 3 weeks after infection.

By combining probes having different fluorophores, we were able to display a large number of active hydrolases in only two labeling reactions on multiple biological replicates. The combination of JJB383 and FP-Tamra displays α-glycosidase and Ser hydrolases using different fluorophores, respectively. Likewise, the combination of JJB70, MV201, and JOPD1 displays the activities of β-glycosidases and Cys proteases using different fluorophores. These experiments displayed remarkably different profiles upon infection, irrespective of the *Fox* isolate used (Supplemental Fig. S5). The activities of both 100-kD putative α-glucosidase and putative β-glucosidases at 50 to 70 kD are increased upon infection (Fig. 8A). By contrast, the activities of one strong 50-kD and several weaker 60-kD Ser hydrolase signals are reduced upon infection (Fig. 8B). Several active β-glucosidases of 45 to 60 kD appear upon infection, while strong signals at 65 and 70 kD disappear (Fig. 8C). Finally, the activity profile of Cys proteases changes dramatically upon infection (Fig. 8D). These signals represent papain-like Cys proteases (MV201; Richau et al., 2012) or vacuolar processing enzymes (JOPD1; Lu et al., 2015). In conclusion, this simple experiment illustrates the ease and potential of investigating the activities of diverse classes of hydrolases using probes having different fluorophores.

DISCUSSION

We have validated activity-based probes for α-glycosidases in plants. We discovered that they label all four members of the GH31 family as well as many additional β-glycosidases that run at a lower molecular mass. The labeling of α-glycosidases is pH dependent and can be suppressed by miglitol and partially by acarbose. Activity profiling of α-glycosidases can be broadly applied to other plants, including nonmodel plant species. We used glycosidase probes to quantify and identify 67 active glycosidases

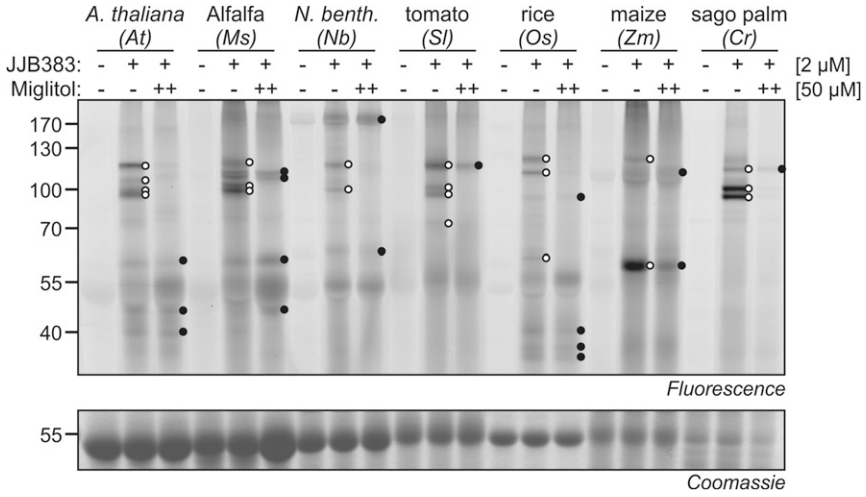

Figure 6. α-Glucosidase profiling in leaves of other plant species. Leaf extracts were preincubated with or without 50 μM miglitol and then labeled with or without 2 μM JJB383 at pH 7 for 1 h. Samples were analyzed by in-gel fluorescence scanning (ex633/em670; top gel) and Coomassie Blue staining (bottom gel). Putative αGH signals are suppressed by miglitol preincubation (white dots), whereas putative βGH signals are not (black dots).

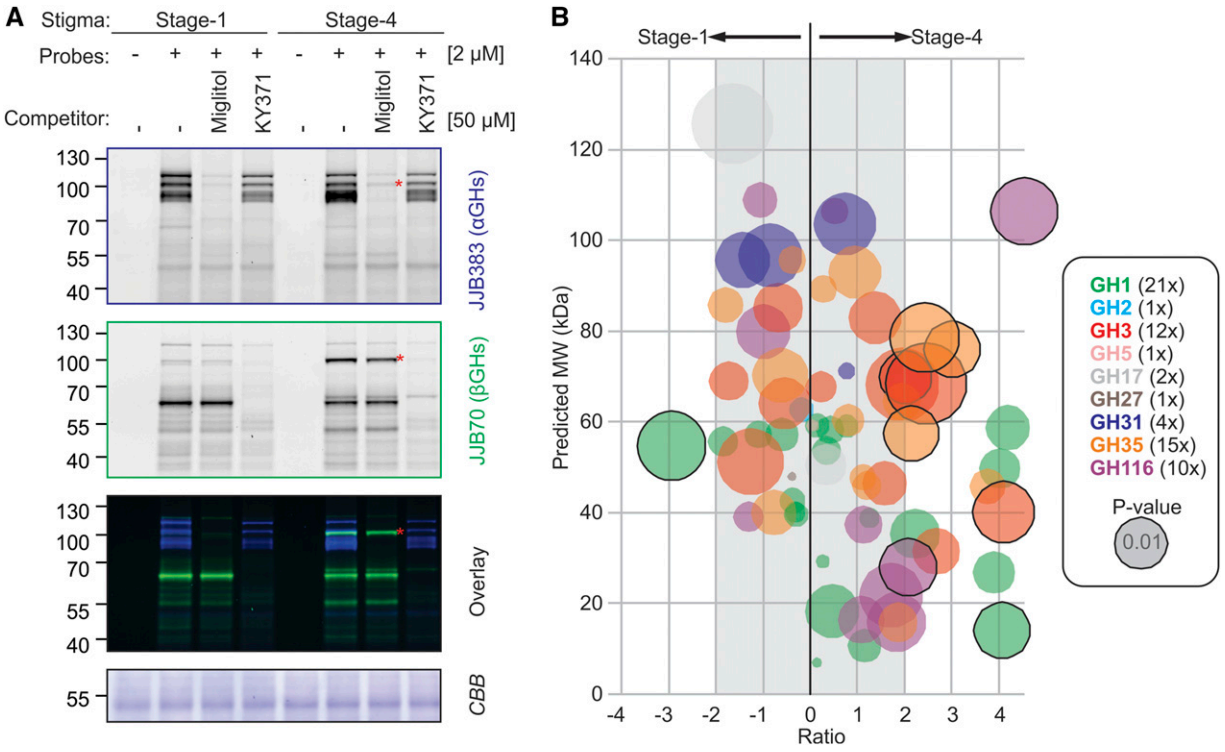

Figure 7. Glucosidase activities in the stigmas of saffron crocus during anthesis. A, Glycosidase activity profiles of stigmas at anthesis stages 1 and 4. Stigma extracts of stages 1 and 4 were preincubated at pH 7 with and without 50 μM miglitol or KY371 for 30 min and then labeled with or without 2 μM JJB383 or JJB70 for 1 h. The JJB383- and JJB70-labeled samples were mixed, separated on protein gels, and analyzed by in-gel fluorescence scanning at ex633/em670 for JJB383 (top gel), ex488/em520 for JJB70 (second gel), and Coomassie Blue (CBB) staining (bottom gel). The overlay (third gel) shows JJB383 labeling in blue and JJB70 labeling in green. B, Comparative glycosidase activity profiling of stages 1 and 4 stigmas of saffron crocus. Stigma extracts of stages 1 and 4 were labeled with or without 5 μM biotinylated probes in triplicate, and biotinylated proteins were purified on avidin beads. On-bead trypsin digests were analyzed using a reannotated proteome of saffron crocus. For each detected GH, the occurrence in the two samples (ratio) was plotted against the predicted molecular mass, with the circle size representing the *P* value and the color indicating the GH family. Ten significantly differential GHs ($P < 0.01$, Student's *t* test) are highlighted with a black edge.

from the stigmas of the saffron crocus. We also used multiplex fluorescence labeling with probes for Ser hydrolases and Cys proteases to display the dynamics of hydrolase activities in crocus corms upon infection with *Fox*.

The Range of Enzymes Labeled by α-Glycosidase Probes

We detected four GH31 α-glycosidases in Arabidopsis, both by in-gel and on-bead digestion of purified biotinylated proteins (Figs. 4 and 5). We also identified the putative orthologs of three of the active GH31 α-glycosidases from the nonmodel plant species saffron crocus (Fig. 7), illustrating the robustness of α-glycosidase activity in different plant species. Although we did not detect XYL2, the gene encoding XYL2 is considered a pseudogene (Iglesias et al., 2006).

It is interesting that, although our probes mimic α-Glc, consistent with the labeling of the α-glucosidases AGLU1 and RSW3, we also label glycosidases that recognize α-Xyl (XYL1) and α-Man (HGL1). These two monosaccharides, however, are relatively similar to Glc. This result indicates that the α-configured cyclophellitol aziridine probes have a degree of promiscuity, allowing them to label a broad range of glycosidases. We made a similar observation for the β-configured cyclophellitol aziridine probes that not only label β-glucosidases but also β-galactosidases, β-xylosidases, β-glucuronidases, and β-glucanases (Chandrasekar et al., 2014).

We did not detect α-glycosidases from other GH families for several reasons. First, the majority of the other α-glycosidases are inverting glycosidases, and these do not covalently react with cyclophellitol aziridine probes. These include the endoplasmic reticulum-resident GCS1 (KNOPF), which catalyzes the first step of *N*-glycan trimming in the folding cycle and is a GH63 inverting α-glycosidase (Boisson et al., 2001). Second, the α-configured cyclophellitol aziridine probe may not be able to enter more specific substrate-binding pockets of α-glycosidases acting on complex glycans. Third, not all α-glycosidases may be expressed in the analyzed

tissues or may not be active under the tested conditions. This condition dependency is illustrated by the fact that the labeling profile depends on pH (Fig. 2).

In addition to α-glycosidases, we also detected the labeling of a large number of β-glycosidases. This result is remarkable because the α-glycosidases were not detected with β-configured probes (Chandrasekar et al., 2014). However, this may be due to the lower concentration of α-glycosidases when compared with β-glycosidases. Nevertheless, the fact that α-configured probes label βGHs, but not vice versa, also has been noted in studies on mammalian proteomes (Jiang et al., 2016), and this property has been used to design more selective αGH inhibitors (Artola et al., 2017). Interestingly, not all β-glycosidases are labeled by α-configured probes. The highly abundant myrosinases TGG1 and TGG2, for example, produce strong labeling signals with β-configured probes (Chandrasekar et al., 2014; Fig. 1B) but are not labeled by the α-configured probes and are not detected by MS.

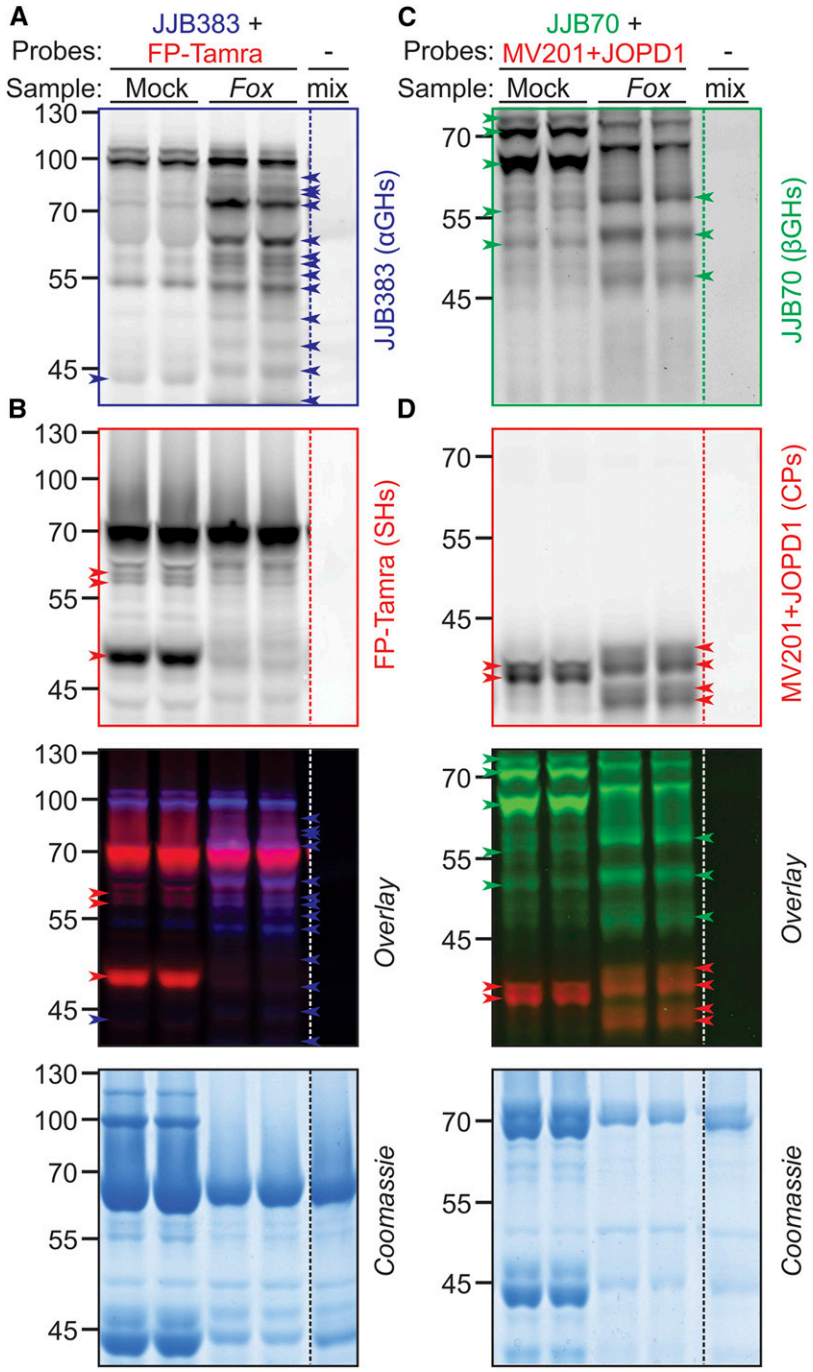

Figure 8. Differential hydrolase activities in saffron corms upon infection with *Fox*. Saffron corms were inoculated with or without four different *Fox* isolates in duplicate (Supplemental Fig. S5), and cell-free extracts were generated and lyophilized after 2 weeks. Extracts were labeled for 4 h in 4 mM DTT at pH 7 with 2 μM JJB383 and FP-Tamra (A and B) or at pH 5 with 2 μM JJB70, MV201, and JOPD1 (C and D). Proteins were separated on protein gels and analyzed by in-gel fluorescence scanning at ex633/em670 to detect JJB383 (A), ex488/em520 to detect JJB70 (C), and ex532/em610 to detect FP-Tamra, MV201, and JOPD1 (B and D). The second and bottom gels show the overlay of JJB383 in blue and FP-Tamra in red (left) and JJB70 in green and MV201 + JOPD1 in red (right) and Coomassie Blue staining (bottom). Shown are the mixed mock and *Fox* samples in duplicate and a mix of the mixed proteomes as a no-probe-control (mix). The activity profiles of separate proteomes are shown in Supplemental Figure S5.

The Identity of the 100- to 130-kD Signals in the α-Glycosidase Activity Profiles

The α-glycosidases cause distinct signals in the 100- to 130-kD region, consistent with their predicted molecular masses (Fig. 4). Unfortunately, the signals are too close to separate and identify the proteins corresponding to each signal. However, we can predict that the bottom signals represent AGLU1 and XYL1 for several reasons. First, this signal also appears upon labeling at pH 4 to 5 (Fig. 2A), consistent with their function in the apoplast. Second, this signal is sensitive to acarbose inhibition (Fig. 3), and AGLU1 is known to be inhibited by acarbose (Frandsen et al., 2000). Third, AGLU1 and XYL1 have the lowest predicted molecular masses (Fig. 5C). Conversely, our data suggest that HGL1 may generate one of the top signals, as it is expected to have the higher molecular mass and to be active in the Golgi (pH 6.5). This result implies that HGL1 may be insensitive to acarbose but not to miglitol inhibition.

α-Glycosidase Activity Profiling Is Broadly Applicable in Plant Science

Our work demonstrates that α-glycosidase activity profiling is broadly applicable. We were able to display miglitol-sensitive labeling of 100- to 130-kD proteins from leaves of monocot and dicot plants and the leaves of a gymnosperm (Fig. 6). These signals very likely represent the orthologs of the Arabidopsis α-glycosidases RSW3, HGL1, AGLU1, and XYL1. Three of these enzymes also were detected upon labeling of saffron crocus anthers (Fig. 5C). We displayed activity profiles of α-glycosidases in leaves, stigmas, and corms (Figs. 6–8), further supporting the broad applicability of this technique. Since the probes are uncharged, and β-configured probes have been used for in vivo labeling (Chandrasekar et al., 2014), we believe that the probes also can be used for the in vivo labeling of α-glycosidases.

We also applied α-glycosidase activity profiling to stigmas and corms of the saffron crocus to study stigma development (Fig. 7) and *Fox* infection (Fig. 8). These experiments illustrate the ease with which α-glycosidase activity profiling can be applied to cash-crop plants to generate data for follow-up studies. For instance, our data suggest candidate glycosidases responsible for the conversion of picrocrocin into safranal in harvested stigmas. Likewise, we detect the suppressed activity of an α-glycosidase upon infection with *Fox*, consistent with the notion that *Fox* is likely to suppress AGLU1 in the apoplast during infection to overcome the antifungal activity of this enzyme (Xiao et al., 1994; Monroe et al., 1999).

Multiplex Fluorescence Activity Profiling Displays Dynamic Changes in Hydrolase Activities

The use of probes having different fluorophores greatly expands the ease with which we can profile multiple classes of hydrolases simultaneously. Multiplex labeling will drastically accelerate research and miniaturize the experiments. By labeling of saffron stigmas and infected corms (Figs. 7A and 8), we have illustrated the ease with which multiplex fluorescence simultaneously displays the activity profiles of different enzyme classes.

The changes in hydrolase activities upon infection of corms by *Fox* are interesting and robust (Fig. 8; Supplemental Fig. S5). The signals that appear in infected corms may be generated by plant-produced hydrolases aimed to suppress the disease or may come from *Fox* itself, to macerate the host tissue (Mohamed et al., 2017). The reduced activity of a 50-kD plant Ser hydrolase upon *Fox* infection may be caused by a depletion of this 50-kD protein but also may be caused by the suppression of the activity of this protein by *Fox*. We have detected a similar suppression of host hydrolase activities upon bacterial infection (Hong and van der Hoorn, 2014; Chandrasekar et al., 2017). The suppression of host enzymes can be studied further using convolution ABPP, where samples from infected and noninfected samples are mixed before and after labeling (Chandrasekar et al., 2017).

In conclusion, we have validated activity profiling for α-glycosidases, showed its broad applicability by profiling other tissues, plant species, and biological phenomena, and introduced multiplex labeling to speed up and miniaturize activity profiling in plant science.

MATERIALS AND METHODS

Probes and Inhibitors

The activity-based probes JJB382, JJB347, JJB383, and JJB384 (Jiang et al., 2016) and JJB70, JJB75, JJB111, and KY371 (Kallemeijn et al., 2012; Chandrasekar et al., 2014) have been described previously. Immunosugars DNJ (Wennekes et al., 2007), DGJ, and *ido*DNJ (Wennekes et al., 2010) have been described previously. Acarbose, miglitol, and galactostatin were purchased from Sigma-Aldrich, Tocris, and Santa Cruz, respectively.

Plant Material, Growth Conditions, and *Fox* Infections

Arabidopsis (*Arabidopsis thaliana*) ecotype Columbia, alfalfa (*Medicago sativa*), *Nicotiana benthamiana*, tomato (*Solanum lycopersicum*), rice (*Oryza sativa*), maize (*Zea mays*), and sago palm (*Cycas revoluta*) were grown on soil under standard greenhouse conditions. Healthy corms of saffron crocus (*Crocus sativus*), previously disinfected with 5% [v/v] sodium hypochlorite for 15 min followed by three washes with sterile water, were planted in sterile substrate and held for 3 weeks with controlled temperature and light (12/12 h of light/dark and 25°C/21°C). The inoculum consisted of a suspension of conidia obtained after 1 week in potato (*Solanum tuberosum*)-Glc medium, stirred at 150 rpm. To remove the mycelium, the suspension was filtered with a double layer of cheesecloth. The conidia suspension was adjusted to 10^5 conidia mL^{-1} and used for the inoculation of plant material. The plant roots were immersed for 24 h in the suspension of conidia (200 mL of suspension), then transplanted back and kept under the same conditions of temperature and light for 3 weeks.

Protein Extraction

Two leaf discs (0.9 cm diameter) were taken from the leaves of various plant species and homogenized with 300 μL of a buffer with suitable pH (50 mM sodium acetate buffer for pH 3 and 4, 50 mM MES buffer for pH 5 and 6, 50 mM MOPS buffer for pH 7 and 8, and 50 mM Tris buffer for pH 9 and 10). After the tissues had been ground in a 1.5-mL tube, the samples were centrifuged at 10,000*g* (4°C for 10 min) followed by 11,000*g* (4°C for 5 min) to remove cell debris, and the supernatant containing soluble proteins was used for labeling.

Labeling Plant Extracts

All probes were prepared as 0.1 to 10 mM stock solutions in dimethyl sulfoxide. Equal volumes of dimethyl sulfoxide were used as a no-probe control. Labeling was performed as described previously (Chandrasekar et al., 2014). For fluorescence gel imaging, the extracts were incubated with 2 μM probes for 1 h at room temperature in the dark at a 50-μL total reaction volume. For the competition experiments, the extracts were preincubated with the corresponding inhibitors at 50 μM for 30 min prior to labeling with the probe.

The labeling reactions were quenched by adding 4× gel loading buffer (200 mM Tris-HCl [pH 6.8], 400 mM DTT, 8% [w/v] SDS, 0.04% [w/v] bromophenol blue, and 40% [v/v] glycerol) at 1× final concentration and heating at 95°C for 5 min. The labeled proteins were separated on 10% protein gels and detected on the protein gels with the Typhoon FLA 9000 scanner at ex488/em520 or ex633/em670 (GE Healthcare Life Sciences). Subsequent to fluorescence imaging, the gels were stained with Coomassie Brilliant Blue R-250. The fluorescence of the labeled proteins was quantified using ImageJ. For pull-down experiments, the extracts from three biological replicates were incubated with 5 μM probes for 1.5 h at room temperature in the dark at a 1-mL total reaction volume. The labeling reactions were quenched by precipitating the total proteins via the chloroform/methanol precipitation method (Wessel and Flugge, 1984).

Pull-Down and On-Bead, In-Gel Trypsin Digestion

Pull-down experiments and on-bead and in-gel trypsin digestions were performed as described with minor modifications (Chandrasekar et al., 2014). For Arabidopsis, healthy leaf discs (1.5 g) were collected from middle/top leaves of 5-week-old Arabidopsis plants growing in different pots at the same point of time. Leaf discs were mixed, and three separate extracts were generated in 50 mM MOPS at pH 7. For saffron crocus sigmas, four stigmas, each from a single flower, were harvested for each stage from different plants of the same age but at different time points. These four stigmas were pooled for the pull-down experiment, and three of these pooled samples were used as biological replicates. The trypsin-digested peptides were purified using Sep-Pak C18 columns (Waters; WAT020515). The columns were equilibrated with 2% (v/v) acetonitrile (ACN) and 0.1% (v/v) formic acid (FA) before peptide loading. Peptides were washed with 10 mL of 2% (v/v) ACN and 0.1% (v/v) FA and eluted with 2 × 1 mL of 65% (v/v) ACN and 0.1% (v/v) FA. Purified peptides were dried in a vacuum centrifuge and subjected to MS analysis. After elution from the Sep-Pak, samples were dried using a vacuum concentrator (Eppendorf), and the peptides were resuspended in 0.1% [v/v] FA solution (15 μL).

LC-MS/MS

Experiments were performed on an Orbitrap Elite instrument (Thermo; Michalski et al., 2012) that was coupled to an EASY-nLC 1000 liquid chromatograph (Thermo). The liquid chromatograph was operated in the one-column mode. The analytical column was a fused silica capillary (75 μm × 20 cm or 75 μm × 40 cm) with an integrated PicoFrit emitter (New Objective) packed in house with Reprosil-Pur 120 C18-AQ 1.9-μm resin (Dr. Maisch). The analytical column was encased by a column oven (Sonation) and attached to a nanospray flex ion source (Thermo). The column oven temperature was adjusted to 45°C during data acquisition and in all other modes at 30°C. The liquid chromatograph was equipped with two mobile phases: solvent A (0.1% [v/v] FA in water) and solvent B (0.1% [v/v] FA in ACN). All solvents were of ultra-performance liquid chromatography grade (Sigma-Aldrich). Peptides were loaded directly onto the analytical column with a maximum flow rate that would not exceed the set pressure limit of 980 bar (usually around 0.6–1 μL min^{-1}). Peptides were subsequently separated on the analytical column by running a 70- or 140-min gradient of solvents A and B (70-min gradient: start with 7% B; gradient 7% to 35% B for 60 min; gradient 35% to 100% B for 5 min; and 100% B for 5 min; 140-min gradient: start with 7% B; gradient 7% to 35% B for 120 min; gradient 35% to 100% B for 10 min; and 100% B for 10 min) at a flow rate of 300 nL min^{-1}. The mass spectrometer was operated using Xcalibur software (version 2.2 SP1.48) and was set in positive ion mode. Precursor ion scanning was performed in the Orbitrap analyzer (Fourier transform mass spectrometry) in the scan range of *m/z* 300 to 1,800 and at a resolution of 60,000 with the internal lock mass option turned on (lock mass was 445.120025 *m/z*, polysiloxane; Olsen et al., 2005). Product ion spectra were recorded in a data-dependent fashion in the ion trap in a variable scan range and at a rapid scan rate. The ionization potential (spray voltage) was set to 1.8 kV. Peptides were analyzed using a repeating cycle consisting of a full precursor ion scan (1×10^6 ions or 50 ms) followed by 12 or 15 product ion scans (1×10^4 ions or 80–100 ms) where peptides are isolated based on their intensity in the full survey scan (threshold of 500 counts) for tandem mass spectrum (MS2) generation that permits peptide sequencing and identification. Collision-induced dissociation energy was set to 35% for the generation of MS2. During MS2 data acquisition, dynamic ion exclusion was set to 60 to 120 s with a maximum list of excluded ions consisting of 500 members and a repeat count of one. Ion injection time prediction, preview mode for Fourier transform mass spectrometry, monoisotopic precursor selection, and charge state screening were enabled. Only charge states of greater than 1 were considered for fragmentation.

Peptide and Protein Identification Using MaxQuant

Spectra (RAW files) were submitted to an Andromeda (Cox et al., 2011) search in MaxQuant (version 1.5.0.25 or 1.5.3.30) using the default settings (Cox and Mann, 2008). Label-free quantification and match-between-runs were activated (Cox et al., 2014). For Arabidopsis samples, the MS2 data were searched against an Arabidopsis (taxonomy identifier 3702) database downloaded from the TAIR repository (TAIR10_pep_20110103.fasta; 27,416 entries). For saffron crocus (taxonomy identifier 82528) samples, we generated a dedicated protein database by translating the publicly available RNA sequencing data from Jain et al. (2016) and filtering for open reading frames that encode proteins of more than 50 amino acids (Supplemental File S1; Saffron.PROTEIN_50.fasta; 83,422 entries). All searches included a contaminants database search (as implemented in MaxQuant; 245 sequences). The contaminants database contains known MS contaminants and was included to estimate the level of contamination. Andromeda searches allowed oxidation of Met residues (16 D) and acetylation of the protein N terminus (42 D) as dynamic modifications and the static modification of Cys (57 D, alkylation with iodoacetamide). Enzyme specificity was set to trypsin/P with two missed cleavages allowed. The instrument type in Andromeda searches was set to Orbitrap, and the precursor mass tolerance was set to ±20 ppm (first search) and ±4.5 ppm (main search). The MS/MS match tolerance was set to ±0.5 D. The peptide spectrum match false discovery rate and the protein false discovery rate were set to 0.01 (based on the target-decoy approach). The minimum peptide length was seven amino acids. For protein quantification, unique and razor peptides were allowed. Modified peptides were allowed for quantification. The minimum score for modified peptides was 40. Label-free protein quantification was switched on, and unique and razor peptides were considered for quantification with a minimum ratio count of 2. Retention times were recalibrated based on the built-in nonlinear time-rescaling algorithm. MS/MS identifications were transferred between LC-MS/MS runs with the match between runs option, in which the maximal match time window was set to 0.7 min and the alignment time window was set to 20 min. The quantification was based on the value at maximum of the extracted ion current. At least two quantification events were required for each protein. Further analysis and filtering of the results were done in Perseus version 1.5.5.3 (Tyanova et al., 2016). Briefly, only protein groups with at least two identified unique peptides over all runs were considered for further analysis. Comparison of protein group quantities (relative quantification) between different MS runs was based solely on the LFQs, as calculated by MaxQuant (MaxLFQ algorithm; Cox et al., 2014). Imputed values were generated over the whole matrix, and the fold change and *P* values were calculated over the three biological replicates.

Open Reading Frame Detection and Domain Annotation

The complete set of de novo assembled transcripts was subject to open reading frame detection using three different prediction algorithms: GeneMarkS-T (Tang et al., 2015), TransDecoder (Haas et al., 2013), and Prodigal (Hyatt et al., 2010). Prodigal was run in both intronless eukaryotic and prokaryotic modes; thus, up to four open reading frame predictions were generated for each transcript. To select the single best open reading frame for each transcript, the following process was applied. If multiple methods predicted overlapping open reading frames, then the longest was chosen. Where multiple methods disagreed on the correct open reading frame, then the following decision process was followed. If all methods disagreed (either in frame or location), then the priority for assignment was taken as GeneMarkS-T, TransDecoder, Prodigal (eukaryotic settings), and Prodigal (prokaryotic settings). If some methods agreed, then the open reading frame that was detected by the largest number of methods was chosen. Only open reading frames of 50 or more amino acids were selected for further analysis. To annotate

conserved domains in the predicted open reading frames, the full PFAM-A database (Finn et al., 2016) was searched against the complete set of open reading frames with an e-value cutoff of 1e-5.

Data Availability

The MS proteomics data have been deposited to the ProteomeXchange Consortium via the PRIDE (Vizcaíno et al., 2016) partner repository with the data set identifier PXD009014. The samples are named as follows: in-gel digests Arabidopsis leaves [ACE0111: bands 1-4 (AH7-9)]; on-bead digest Arabidopsis leaves [ACE0149: JJB384 (AH2,5,8) and no-probe control (AH1,4,7)]; and on-bead digest saffron stigma [ACE0158: Stage-1 (AS13-15), Stage-4 (AS3-6), and no-probe control (AS1-3)].

Accession Numbers

Accession numbers are as follows: At5g11720 (AGLU1), At5g63840 (RSW3/PSL5), At3g23640 (HGL1), At1g68560 (XYL1), At4g10060 (GH116), At2g44450 (BGLU15), At1g26560 (BGLU40), At5g36890 (BGLU42), At3g18080 (BHLU44), At3g47000 (F13I12), At5g20950 (BGLC1), and At5g04885 (BGLC3).

Supplemental Data

The following supplemental materials are available.

Supplemental Figure S1. Structures of the probes used.

Supplemental Figure S2. Activity profiles of α- and β-glucosidase probes.

Supplemental Figure S3. Subsequent labeling of α- and β-glucosidases.

Supplemental Figure S4. Duplicate of the pH course.

Supplemental Figure S5. Replicates of *Fox* infection of saffron corms.

Supplemental File S1. The saffron protein database.

ACKNOWLEDGMENTS

We thank Ursula Pyzio for excellent plant care.

Received March 2, 2018; accepted March 6, 2018; published March 19, 2018.

LITERATURE CITED

Ahrazem O, Rubio-Moraga A, Nebauer SG, Molina RV, Gómez-Gómez L (2015) Saffron: its phytochemistry, developmental processes, and biotechnological prospects. J Agric Food Chem **63:** 8751–8764

Andriotis VME, Rejzek M, Barclay E, Rugen MD, Field RA, Smith AM (2016) Cell wall degradation is required for normal starch mobilisation in barley endosperm. Sci Rep **6:** 33215

Artola M, Wu L, Ferraz MJ, Kuo CL, Raich L, Breen IZ, Offen WA, Codée JDC, van der Marel GA, Rovira C, et al (2017) 1,6-Cyclophellitol cyclosulfates: a new class of irreversible glycosidase inhibitor. ACS Cent Sci **3:** 784–793

Boisson M, Gomord V, Audran C, Berger N, Dubreucq B, Granier F, Lerouge P, Faye L, Caboche M, Lepiniec L (2001) Arabidopsis glucosidase I mutants reveal a critical role of N-glycan trimming in seed development. EMBO J **20:** 1010–1019

Cappelli C (1994) Occurrence of *Fusarium oxysporum* f. sp. *gladioli* on saffron in Italy. Phytopathol Mediterr **33:** 93–94

Carrascosa JM, Molero JC, Fermín Y, Martínez C, Andrés A, Satrústegui J (2001) Effects of chronic treatment with acarbose on glucose and lipid metabolism in obese diabetic Wistar rats. Diabetes Obes Metab **3:** 240–248

Chandrasekar B, Colby T, Emran Khan Emon A, Jiang J, Hong TN, Villamor JG, Harzen A, Overkleeft HS, van der Hoorn RAL (2014) Broad-range glycosidase activity profiling. Mol Cell Proteomics **13:** 2787–2800

Chandrasekar B, Hong TN, van der Hoorn RAL (2017) Inhibitor discovery by convolution ABPP. Methods Mol Biol **1491:** 47–56

Costantino HR, Brown SH, Kelly RM (1990) Purification and characterization of an α-glucosidase from a hyperthermophilic archaebacterium, *Pyrococcus furiosus*, exhibiting a temperature optimum of 105 to 115°C. J Bacteriol **172:** 3654–3660

Coutinho PM, Henrissat B (1999) Carbohydrate-active enzymes: an integrated approach. *In* HJ Gilbert, GJ Davies, B Svensson, B Henrissat, eds, Recent Advances in Carbohydrate Engineering. Royal Society of Chemistry, Cambridge, UK, pp 3–12

Cox J, Hein MY, Luber CA, Paron I, Nagaraj N, Mann M (2014) Accurate proteome-wide label-free quantification by delayed normalization and maximal peptide ratio extraction, termed MaxLFQ. Mol Cell Proteomics **13:** 2513–2526

Cox J, Mann M (2008) MaxQuant enables high peptide identification rates, individualized p.p.b.-range mass accuracies and proteome-wide protein quantification. Nat Biotechnol **26:** 1367–1372

Cox J, Neuhauser N, Michalski A, Scheltema RA, Olsen JV, Mann M (2011) Andromeda: a peptide search engine integrated into the MaxQuant environment. J Proteome Res **10:** 1794–1805

Cravatt BF, Wright AT, Kozarich JW (2008) Activity-based protein profiling: from enzyme chemistry to proteomic chemistry. Annu Rev Biochem **77:** 383–414

Finn RD, Coggill P, Eberhardt RY, Eddy SR, Mistry J, Mitchell AL, Potter SC, Punta M, Qureshi M, Sangrador-Vegas A, et al (2016) The Pfam protein families database: towards a more sustainable future. Nucleic Acids Res **44:** D279–D285

Frandsen TP, Lok F, Mirgorodskaya E, Roepstorff P, Svensson B (2000) Purification, enzymatic characterization, and nucleotide sequence of a high-isoelectric-point α-glucosidase from barley malt. Plant Physiol **123:** 275–286

Gershater MC, Cummins I, Edwards R (2007) Role of a carboxylesterase in herbicide bioactivation in Arabidopsis thaliana. J Biol Chem **282:** 21460–21466

Gu C, Kolodziejek I, Misas-Villamil J, Shindo T, Colby T, Verdoes M, Richau KH, Schmidt J, Overkleeft HS, van der Hoorn RAL (2010) Proteasome activity profiling: a simple, robust and versatile method revealing subunit-selective inhibitors and cytoplasmic, defense-induced proteasome activities. Plant J **62:** 160–170

Gu C, Shannon DA, Colby T, Wang Z, Shabab M, Kumari S, Villamor JG, McLaughlin CJ, Weerapana E, Kaiser M, et al (2013) Chemical proteomics with sulfonyl fluoride probes reveals selective labeling of functional tyrosines in glutathione transferases. Chem Biol **20:** 541–548

Haas BJ, Papanicolaou A, Yassour M, Grabherr M, Blood PD, Bowden J, Couger MB, Eccles D, Li B, Lieber M, et al (2013) *De novo* transcript sequence reconstruction from RNA-seq using the Trinity platform for reference generation and analysis. Nat Protoc **8:** 1494–1512

Hillman RJ, Scott M, Gray RS (1989) Effect of alpha-glucosidase inhibition on glucose profiles in insulin dependent diabetes. Diabetes Res **10:** 81–84

Hong TN, van der Hoorn RAL (2014) DIGE-ABPP by click chemistry: pairwise comparison of serine hydrolase activities from the apoplast of infected plants. Methods Mol Biol **1127:** 183–194

Husaini AM (2014) Challenges of climate change: omics-based biology of saffron plants and organic agricultural biotechnology for sustainable saffron production. GM Crops Food **5:** 97–105

Hyatt D, Chen GL, Locascio PF, Land ML, Larimer FW, Hauser LJ (2010) Prodigal: prokaryotic gene recognition and translation initiation site identification. BMC Bioinformatics **11:** 119

Iglesias N, Abelenda JA, Rodiño M, Sampedro J, Revilla G, Zarra I (2006) Apoplastic glycosidases active against xyloglucan oligosaccharides of *Arabidopsis thaliana*. Plant Cell Physiol **47:** 55–63

Jain M, Srivastava PL, Verma M, Ghangal R, Garg R (2016) *De novo* transcriptome assembly and comprehensive expression profiling in *Crocus sativus* to gain insights into apocarotenoid biosynthesis. Sci Rep **6:** 22456

Jiang J, Kuo CL, Wu L, Franke C, Kallemeijn WW, Florea BI, van Meel E, van der Marel GA, Codée JDC, Boot RG, et al (2016) Detection of active mammalian GH31 α-glucosidases in health and disease using in-class, broad-spectrum activity-based probes. ACS Cent Sci **2:** 351–358

Kallemeijn WW, Li KY, Witte MD, Marques ARA, Aten J, Scheij S, Jiang J, Willems LI, Voorn-Brouwer TM, van Roomen CPAA, et al (2012) Novel activity-based probes for broad-spectrum profiling of retaining β-exoglucosidases in situ and in vivo. Angew Chem Int Ed Engl **51:** 12529–12533

Kaschani F, Gu C, Niessen S, Hoover H, Cravatt BF, van der Hoorn RAL (2009) Diversity of serine hydrolase activities of unchallenged and Botrytis-infected *Arabidopsis thaliana*. Mol Cell Proteomics **8:** 1082–1093

Kolodziejek I, Misas-Villamil JC, Kaschani F, Clerc J, Gu C, Krahn D, Niessen S, Verdoes M, Willems LI, Overkleeft HS, et al (2011) Proteasome activity imaging and profiling characterizes bacterial effector syringolin A. Plant Physiol **155:** 477–489

Krammer G, Winterhalter P, Schwab M, Shreier P (2002) Glycosidically bound aroma compounds in the fruits of *Prunus* species: apricot (*P. armeniaca* L.), peach (*P. persica* L.), yellow plum (*P. domestica* L. ssp. *syriaca*). Postharvest Biol Technol **39:** 778–781

Lenger J, Kaschani F, Lenz T, Dalhoff C, Villamor JG, Köster H, Sewald N, van der Hoorn RAL (2012) Labeling and enrichment of *Arabidopsis thaliana* matrix metalloproteases using an active-site directed, marimastat-based photoreactive probe. Bioorg Med Chem **20:** 592–596

Lombard V, Golaconda Ramulu H, Drula E, Coutinho PM, Henrissat B (2014) The Carbohydrate-Active Enzymes database (CAZy) in 2013. Nucleic Acids Res **42:** D490–D495

Lu H, Chandrasekar B, Oeljeklaus J, Misas-Villamil JC, Wang Z, Shindo T, Bogyo M, Kaiser M, van der Hoorn RAL (2015) Subfamily-specific fluorescent probes for cysteine proteases display dynamic protease activities during seed germination. Plant Physiol **168:** 1462–1475

Martínez DE, Bartoli CG, Grbic V, Guiamet JJ (2007) Vacuolar cysteine proteases of wheat (*Triticum aestivum* L.) are common to leaf senescence induced by different factors. J Exp Bot **58:** 1099–1107

Michalski A, Damoc E, Lange O, Denisov E, Nolting D, Müller M, Viner R, Schwartz J, Remes P, Belford M, et al (2012) Ultra high resolution linear ion trap Orbitrap mass spectrometer (Orbitrap Elite) facilitates top down LC MS/MS and versatile peptide fragmentation modes. Mol Cell Proteomics **11:** O111.013698

Misas-Villamil JC, Toenges G, Kolodziejek I, Sadaghiani AM, Kaschani F, Colby T, Bogyo M, van der Hoorn RAL (2013) Activity profiling of vacuolar processing enzymes reveals a role for VPE during oomycete infection. Plant J **73:** 689–700

Misas-Villamil JC, van der Burgh AM, Grosse-Holz F, Bach-Pages M, Kovács J, Kaschani F, Schilasky S, Emon AE, Ruben M, Kaiser M, et al (2017) Subunit-selective proteasome activity profiling uncovers uncoupled proteasome subunit activities during bacterial infections. Plant J **90:** 418–430

Mohamed MSM, Saleh AM, Abdel-Farid IB, El-Naggar SA (2017) Growth, hydrolases and ultrastructure of *Fusarium oxysporum* as affected by phenolic rich extracts from several xerophytic plants. Pestic Biochem Physiol **141:** 57–64

Monroe JD, Gough CM, Chandler LE, Loch CM, Ferrante JE, Wright PW (1999) Structure, properties, and tissue localization of apoplastic α-glucosidase in crucifers. Plant Physiol **119:** 385–397

Morimoto K, van der Hoorn RAL (2016) The increasing impact of activity-based protein profiling in plant science. Plant Cell Physiol **57:** 446–461

Mueller AN, Ziemann S, Treitschke S, Aßmann D, Doehlemann G (2013) Compatibility in the *Ustilago maydis*-maize interaction requires inhibition of host cysteine proteases by the fungal effector Pit2. PLoS Pathog **9:** e1003177

Olsen JV, de Godoy LM, Li G, Macek B, Mortensen P, Pesch R, Makarov A, Lange O, Horning S, Mann M (2005) Parts per million mass accuracy on an Orbitrap mass spectrometer via lock mass injection into a C-trap. Mol Cell Proteomics **4:** 2010–2021

Palmero D, Rubio-Moraga A, Galvez-Paron L, Nogueras J, Abato C, Gomez-Gomez L, Ahrazem O (2014) Pathogenicity and genetic diversity of *Fusarium oxysporum* isolates from corms of *Crocus sativus*. Ind Crops Prod **61:** 186–192

Richau KH, Kaschani F, Verdoes M, Pansuriya TC, Niessen S, Stüber K, Colby T, Overkleeft HS, Bogyo M, van der Hoorn RA (2012) Subclassification and biochemical analysis of plant papain-like cysteine proteases displays subfamily-specific characteristics. Plant Physiol **158:** 1583–1599

Sadler NC, Wright AT (2015) Activity-based protein profiling of microbes. Curr Opin Chem Biol **24:** 139–144

Stanley D, Rejzek M, Naested H, Smedley M, Otero S, Fahy B, Thorpe F, Nash RJ, Harwood W, Svensson B, et al (2011) The role of α-glucosidase in germinating barley grains. Plant Physiol **155:** 932–943

Stiti N, Chandrasekar B, Strubl L, Mohammed S, Bartels D, van der Hoorn RAL (2016) Nicotinamide cofactors suppress active-site labeling of aldehyde dehydrogenases. ACS Chem Biol **11:** 1578–1586

Tang S, Lomsadze A, Borodovsky M (2015) Identification of protein coding regions in RNA transcripts. Nucleic Acids Res **43:** e78

Teper-Bamnolker P, Buskila Y, Belausov E, Wolf D, Doron-Faigenboim A, Ben-Dor S, van der Hoorn RAL, Lers A, Eshel D (2017) Vacuolar processing enzyme activates programmed cell death in the apical meristem inducing loss of apical dominance. Plant Cell Environ **40:** 2381–2392

Tyanova S, Temu T, Sinitcyn P, Carlson A, Hein MY, Geiger T, Mann M, Cox J (2016) The Perseus computational platform for comprehensive analysis of (prote)omics data. Nat Methods **13:** 731–740

Verhelst SH, Bogyo M (2005) Chemical proteomics applied to target identification and drug discovery. Biotechniques **38:** 175–177

Vizcaíno JA, Csordas A, del-Toro N, Dianes JA, Griss J, Lavidas I, Mayer G, Perez-Riverol Y, Reisinger F, Ternent T, et al (2016) 2016 update of the PRIDE database and its related tools. Nucleic Acids Res **44:** D447–D456

Wafai AH, Bukhari S, Mokhdomi TA, Amin A, Wani Z, Hussaini A, Mir JI, Qadri RA (2015) Comparative expression analysis of senescence gene *CsNAP* and B-class floral development gene *CsAP3* during different stages of flower development in saffron (*Crocus sativus* L.). Physiol Mol Biol Plants **21:** 459–463

Wennekes T, Meijer AJ, Groen AK, Boot RG, Groener JE, van Eijk M, Ottenhoff R, Bijl N, Ghauharali K, Song H, et al (2010) Dual-action lipophilic iminosugar improves glycemic control in obese rodents by reduction of visceral glycosphingolipids and buffering of carbohydrate assimilation. J Med Chem **53:** 689–698

Wennekes T, van den Berg RJ, Donker W, van der Marel GA, Strijland A, Aerts JM, Overkleeft HS (2007) Development of adamantan-1-yl-methoxy-functionalized 1-deoxynojirimycin derivatives as selective inhibitors of glucosylceramide metabolism in man. J Org Chem **72:** 1088–1097

Wessel D, Flügge UI (1984) A method for the quantitative recovery of protein in dilute solution in the presence of detergents and lipids. Anal Biochem **138:** 141–143

Willems LI, Overkleeft HS, van Kasteren SI (2014) Current developments in activity-based protein profiling. Bioconjug Chem **25:** 1181–1191

Xiao J, Ohshima A, Kamakura T, Ishiyama T, Yamaguchi I (1994) Extracellular glycoprotein(s) associated with cellular differentiation in *Magnaporta grisea*. Mol Plant Microbe Interact **7:** 639–644